Journal of Power Sources 407 (2018) 173–179

Contents lists available at ScienceDirect

Journal of Power Sources

journal homepage: www.elsevier.com/locate/jpowsour

Long cycle life of sodium-ion pouch cell achieved by using multiple electrolyte additives

Haiying Che[a], Xinrong Yang[a], Hong Wang[a], Xiao-Zhen Liao[a,*], Sheng S. Zhang[b], Chunsheng Wang[c], Zi-Feng Ma[a,**]

[a] Shanghai Electrochemical Energy Devices Research Center, Department of Chemistry and Chemical Engineering, Shanghai Jiao Tong University, Shanghai, 200240, China
[b] Electrochemistry Branch, Power and Energy Division Sensor and Electron Devices Directorate, U.S. Army Research Laboratory, Adelphi, MD, 20783, USA
[c] Department of Chemical and Biomolecular Engineering, University of Maryland, College Park, MD, 20740, USA

HIGHLIGHTS

- Long cycle life of sodium-ion pouch cells is obtained by using optimized electrolyte.
- Multiple additives electrolyte is for the $Na_xNi_{1/3}Fe_{1/3}Mn_{1/3}O_2$//hard carbon system.
- The capacity retention of cells comes up to 92% after 1000 cycles.
- SEI on the anode and CEI on the cathode are forming to protect electrodes.

ARTICLE INFO

Keywords:
Sodium-ion battery
Pouch cell
Electrolyte additive
Hard carbon
$Na_xNi_{1/3}Fe_{1/3}Mn_{1/3}O_2$

ABSTRACT

Sodium-ion pouch cells with up to 1000 cycles are presented by using a $NaNi_{1/3}Fe_{1/3}Mn_{1/3}O_2$ cathode, a hard carbon anode, and a functional electrolyte. The functional electrolyte is composed of 1 M $NaPF_6$ dissolved in a 1:1 (v/v) mixed solvent of propylene carbonate (PC) and ethyl methyl carbonate (EMC) with 3–4 wt% of two or three additives, including fluoroethylene carbonate (FEC), prop-1-ene-1,3-sultone (PST), and 1,3,2-Dioxathiolane-2,2-dioxide (DTD). It is shown that the capacity retentions of the cells increase to 84.4% and 92.2% after 1000 cycles for electrolytes containing FEC-PST bi-additive and FEC-PST-DTD tri-additive, respectively, as compared with that containing FEC single additive. Using X-ray photoelectron spectroscopy, inductively coupled plasma optical, and transmission electron microscopy, post-mortem analyses on the surface of the cycled electrodes indicate that PST and DTD are beneficial to the anode by forming an organic compound rich solid electrolyte interphase (SEI), and to the cathode by forming a dense and thick cathode electrolyte interphase (CEI) that consequently prevents transition metal ions from dissolving into electrolyte.

1. Introduction

Sodium-ion batteries (SIBs) are attractive to replace lithium-ion batteries for applications in large-scale electrochemical energy storage due to abundant resource and low cost of sodium [1–5]. Up to date, numerous cathode materials have been reported for SIBs, including Prussian blue analogs [6], layered-structured sodium metal oxides [7–10], and polyanion materials [11–13]. Most of the materials are evaluated by the half-coin cell using Na metal as an anode and an unoptimized electrolyte. The sodium-ion full cell earliest reported by Barker et al. [14] was based on a $NaVPO_4F$/hard-carbon system and 1 M $NaClO_4$/EC + DMC (2:1 by weight) electrolyte, and such a cell lost more than 50% capacity only after 30 cycles. Later, a $Na_3V_2(PO_4)_2F_3$/hard-carbon cell with 1 M Na-salt EC/PC/DMC (45:45:10, v/v) electrolyte was reported to be able to cycle for 120 times [15], and a $Na_4Co_3(PO_4)_2P_2O_7$/hard-carbon cell with 1 M $NaPF_6$/EC + DEC (1:1, v/v) electrolyte retained 83% of initial capacity after 100 cycles [16]. Study on a $NaNi_{0.5}Mn_{0.5}O_2$/hard-carbon cell showed that the SIB's performance was significantly affected by the salts of electrolyte [17]. Toward commercialization, the SIBs still face numerous challenges, not only in the materials but also in the compatibility between materials including both electrodes and electrolyte [18].

Electrolyte profoundly affects the SIBs' performance through interaction between the electrolyte and electrodes in every electrochemical

* Corresponding author.
** Corresponding author.
E-mail addresses: Liaoxz@sjtu.edu.cn (X.-Z. Liao), zfma@sjtu.edu.cn (Z.-F. Ma).

https://doi.org/10.1016/j.jpowsour.2018.08.025
Received 12 May 2018; Received in revised form 19 July 2018; Accepted 9 August 2018
Available online 16 August 2018
0378-7753/

process [19]. In this regard, electrolyte additives have been proven to be very effective in enhancing the compatibility between the electrolyte and electrode materials, and it is found that fluorinated carbonate solvents play important roles in promoting the formation of stable solid electrolyte interphase (SEI) on the anode [20]. In particular, fluoroethylene carbonate (FEC, see structure below) has been widely used as the electrolyte additive for lithium and sodium ion batteries [21–27] because of its slightly higher reduction potential than the common propylene carbonate (PC) solvent, which allows it reducing first to form SEI.

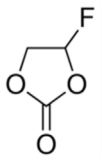

Fluoroethylene carbonate
4-Fluoro-1,3-dioxolan-2-one
(FEC)

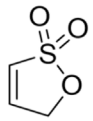

Propene sulfone
Prop-1-ene-1,3-sultone
(PST)

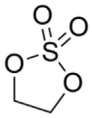

Ethylene sulfate or
1,3,2-Dioxathiolane-2,2-dioxide
(DTD)

In the same principle, it was reported that prop-1-ene-1,3-sultone (PST) [28] and ethylene sulfate (DTD) [29,30] are able to suppress impedance growth of the lithium-ion batteries. Beside the above organic compounds, inorganic rubidium and cesium salts were reported to be capable of modifying the chemical composition of SEI on hard carbon surfaces in sodium-ion batteries [31].

Most of the previous publications on sodium-ion cells were based on the results of coin cells. Due to the limitation of coin cells, some engineering problems such as battery swelling, electrode wettability, and performance degradation cannot be well understood. For this reason, in this work, we synthesized $NaNi_{1/3}Fe_{1/3}Mn_{1/3}O_2$ (NFM) in kilogram scale and assembled 1-Ah sodium-ion pouch cells. It is shown that the pouch cells retain 92.2% of initial capacity after 1000 cycles when using the electrolyte with FEC-PST-DTD tri-additive. In this paper, the effect of PST and DTD on SIB's cycling performance and chemistry of the surfaces on the anode and cathode will be characterized and discussed by the X-ray photoelectron spectroscopy (XPS), inductively coupled plasma atomic emission spectroscopy (ICP-AES) and transmission electron microscopy (TEM) techniques.

2. Experimental

2.1. Electrolyte preparation

A solution of 1 M $NaPF_6$ dissolved in a 1:1 (v/v) mixed solvent of propylene carbonate (PC) and ethyl methyl carbonate (EMC) (1:1 v/v) with 2 wt% FEC was used as the standard electrolyte and donated to F. Using PST and DTD as the second or third additive, the electrolyte containing 2 wt% FEC and 1 wt% PST was prepared and donated to FP, and that containing 2 wt% FEC, 1 wt% PST and 1 wt% DTD was donated to FPD.

2.2. Assembly of pouch cell

NFM cathode material was synthesized in kilogram scale by a co-precipitation and calcination method as reported previously [32]. Pouch cells were assembled using an NFM cathode (120 mAh g^{-1} at 0.1C), a hard carbon (HC, 290 mAh g^{-1} at 0.05C) anode, and a Celgard 2700 membrane as the separator. The NFM and HC slurries were respectively coated onto an Al foil in the ratio of 92 wt% active material, 4 wt% super P, and 4 wt% polyvinylidene fluoride (PVDF) in N-Methyl-2-pyrrolidone (NMP). Areal loading of the anode and cathode were 130 g m^{-2} and 260 g m^{-2}, respectively. The cathode-separator-anode assembles were first prepared, and then stacked with 10 cathode electrodes by 11 anode electrodes and packaged in a plastic-laminated aluminum pouch. Resultant pouch cell was dried under vacuum at 80 °C for 48 h before being moved into a glove box for injecting electrolyte. The size of prepared pouch cells was 52 × 5 × 100 mm (LxWxH).

2.3. Test of electrochemical performance

Before testing, the pouch cells were subjected to a series of pre-processes, consisting of overnight aging and pre-formation at room temperature from open circuit voltage (OCV) to 4.0 V at 20 mA, followed by aging at 45 °C for 24 h, degassing, and vacuum sealing. Cycling test was conducted on a battery test system (CT-4008-5V3A-FA model, Neware Technology Co., Ltd.) by charging at 1 A to 3.8 V and then holding at 3.8 V until the current drops to 20 mA, and discharging at 1 A to 2.0 V.

2.4. Characterization of electrode surface

After cycling test (1000 cycles), the electrodes were harvested, rinsed with EMC solvent, and dried in the glove box. Surface chemistry and depth-profile of the cycled electrodes were characterized by an X-ray photoelectron spectrometer (Kratos Axis Ultra DLD). Surface morphology of the electrodes was observed using a digital camera, a field-emission scanning electron microscope (F-SEM, Sirion 200), and a transmission electron microscope (TEM, JEM-2100), respectively. The grey materials on the surface of the anode were characterized by Energy Dispersive X-Ray analyzer (EDX). Content of transition metal ions in the cycled HC anode was collected by soaking 20 mg active material in 4 g EMC solvent at 55 °C for 7 days and then was determined by an inductively coupled plasma atomic emission spectroscopy. (ICP-AES, Icap 7600).

3. Results and discussion

The cycling performance of pouch cells with different additives is shown in Fig. 1a. It can be found that the additive has a profound influence on the cycle life of pouch cells. The cell using FEC single additive (F) has only 76.6% of capacity retention after 750 cycles. In contrast, the cell using FEC-PST bi-additive (FP) retains 84.4% of initial capacity even after 1000 cycles, and the one using FEC-PST-DTD tri-additive (FPD) further increases to 92.2% of capacity retention after 1000 cycles. Fig. 1b–d compare the charging and discharging voltage profiles of three cells with different additives at 1st, 250^{th}, 750^{th} cycle, respectively. In the 1st cycle (Fig. 1b), all three cells have the same capacity (~0.95 Ah) and voltage profile, meaning that these cells start

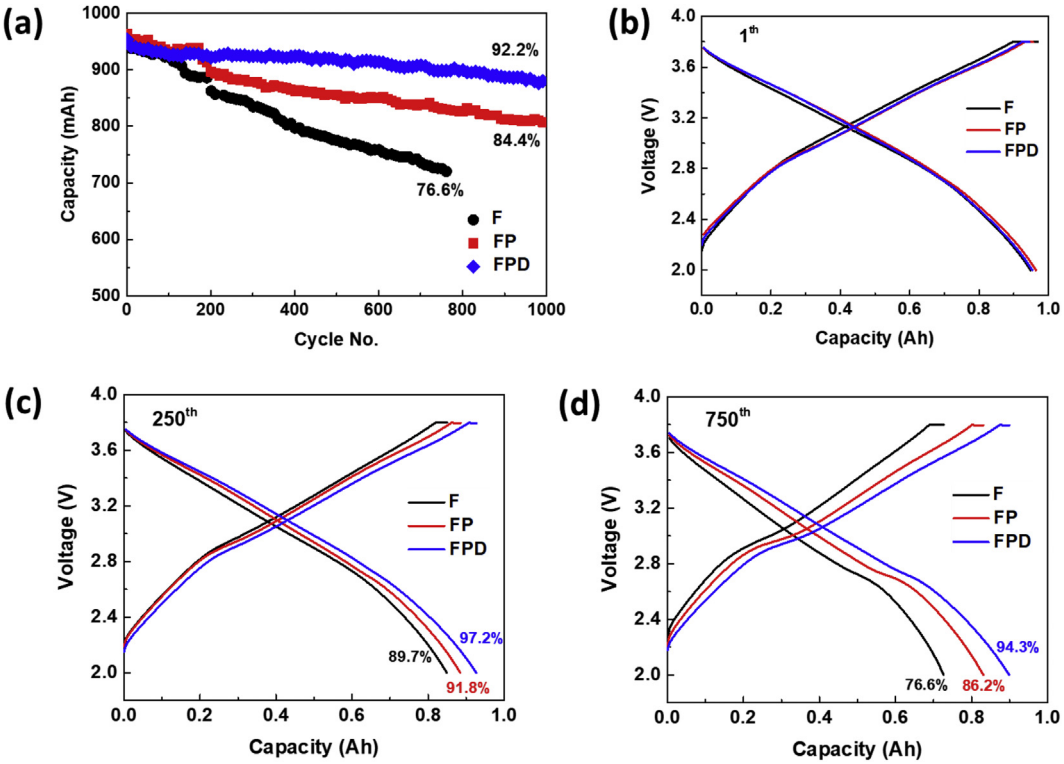

Fig. 1. Effect of electrolyte additive on cycling performance of HC/NFM pouch cell. (a) Capacity retention cycled at 1C between 2.0 V and 3.8 V, (b) voltage profile in the 1st cycle, (c) voltage profile in the 250th cycle, and (d) voltage profile in the 750th cycle.

with the same conditions. With increasing of the cycle number, the differences in the capacity and voltage polarization of the cells are gradually increased, as indicated by Fig. 1c and d. That is, the capacity and discharging voltage are increased in the order of tri-additive > bi-additive > single additive. All the results above indicate that multiple additives are advantageous over the FEC single additive.

After cycling test, morphology and surface chemistry of the cycled electrodes are characterized. Fig. 2 shows digital photos and SEM images of the cycled anodes for three electrolytes of F, FP, and FPD. In the digital photos (top row), grey color matters are visually visible, especially in Fig. 2a as indicated by the small circles. In particular, the amount of grey matters decreases in the order of single additive F > bi-additive FP > tri-additive FPD. The anode cycled with tri-additive FPD has the minimum amount of grey matters, which is attributed to a robust SEI. When exposed to air, the grey matter quickly turned to white color, as shown by comparing Fig. 3a and Fig. 3b. These grey matters are believed to be a mixture of the dead sodium and the product of its reaction with the electrolyte solvents. This judgment was supported by the EDX result showing that the grey matter was mainly composed of O and Na, as suggested in Fig. 3c. In the present case, the dissolution of transition metal ions from the NFM cathode (to be discussed later) would be the major cause for the observed deposition of sodium metal. The dissolved transition metal ions migrate to and deposit on the surface of HC anode, and the resulting transition metals subsequently serve

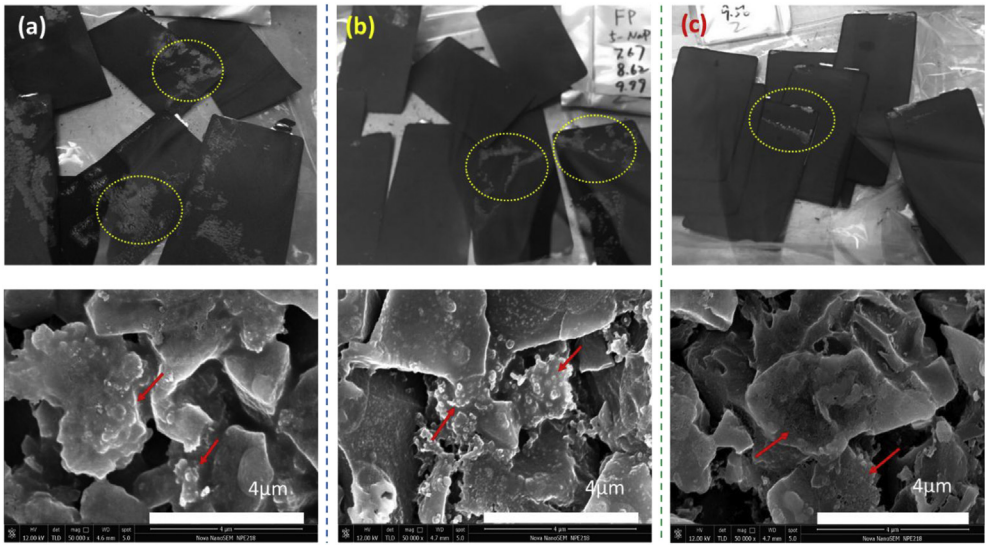

Fig. 2. Digital photo (top row) and SEM image (bottom row) of cycled HC anodes. (a) Single additive F, (b) bi-additive FP, and (c) tri-additive FPD.

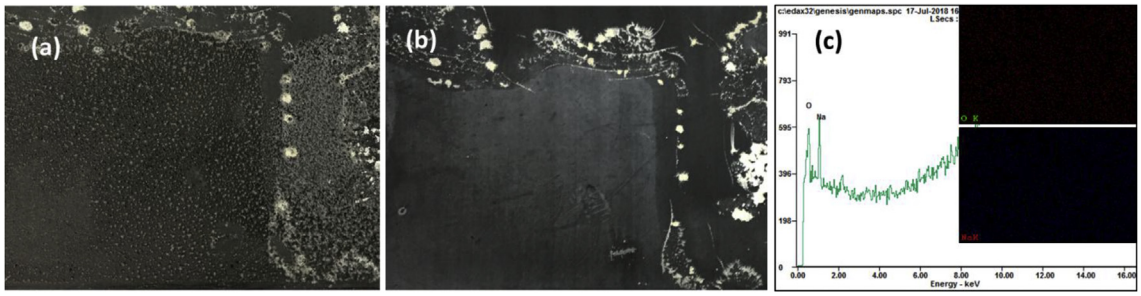

Fig. 3. (a) Digital photo of cycled HC anode in the glove box after EMC solvent cleaning, (b) digital photo of the same anode under the air, (c) EDX result of the white compound on anode surface.

as the seed of the further solvent decomposition and sodium electrodeposition. Same trend in the change of roughness of HC particles is also observed from the SEM images (bottom row), showing that the HC particles with FEC single additive are covered by a number of small particles, namely the solvent decomposition products, while those with the FEC-PST bi-additive and FEC-PST-DTD tri-additive are much clean and smooth. The above observations suggest that cycling performance of the SIBs is affected not only by the deposition of sodium metal and resultant reaction with the electrolyte solvents but also by the decomposition (reduction) of electrolyte solvents on the HC anode. It is important to find that bi- or tri-additives are much more effective in suppressing these two undesired phenomena.

In order to understand the role of additives in improving the cycling performance of the SIBs, the surface of the cycled anode is analyzed by XPS and the results are shown in Fig. 4. It can be seen in Fig. 4a that the surface generally contains Na, F, O, C, P, and S elements, which are originated from the electrolyte, additive, HC, and binder. Spectra of C1s, F1s, and S2p are in detail shown in Fig. 4b–d. In the C1s spectrum (Fig. 4b), there are five types of carbon, including C-H (284.7 eV), C-O (286.2eV), C=O (or O-C-O) (288 eV), O-C=O (289 eV) and $ROCO_2Na$ (or Na_2CO_3) (289–289.8 eV) [33,34]. A significant change associated with the additive is that the relative intensity of the peak at 289.8 eV (corresponding to $ROCO_2Na/Na_2CO_3$) to the peak at 289 eV (O-C=O) is increased by use of the bi- and tri-additives. In other words, the PST and DTD additives promote the formation of $ROCO_2Na$ and Na_2CO_3 salts. In the F1s spectrum (Fig. 4c), there are two major peaks at 684.5eV (anionic F) and at 687.5 eV (co-valent F). It is evident that the bi- and tri-additives greatly increase the relative intensity of covalent F to anionic F, that is, their presence favors the formation covalent F in the SEI. In the S2p spectrum (Fig. 4d), there are three major peaks at 167.2 eV (Na_2SO_3), 169 eV ($ROSO_2Na$), and 170.4 eV (RSO_3Na), respectively, for two anodes cycled with the bi- and tri-additives while having no any S2p signals in the anode cycled with the FEC single additive. This observation reveals that both PST and DTD additives are participated in the formation of SEI, and contribute to the increased stability of SEI.

Morphology of the cycled NFM cathode was further observed by

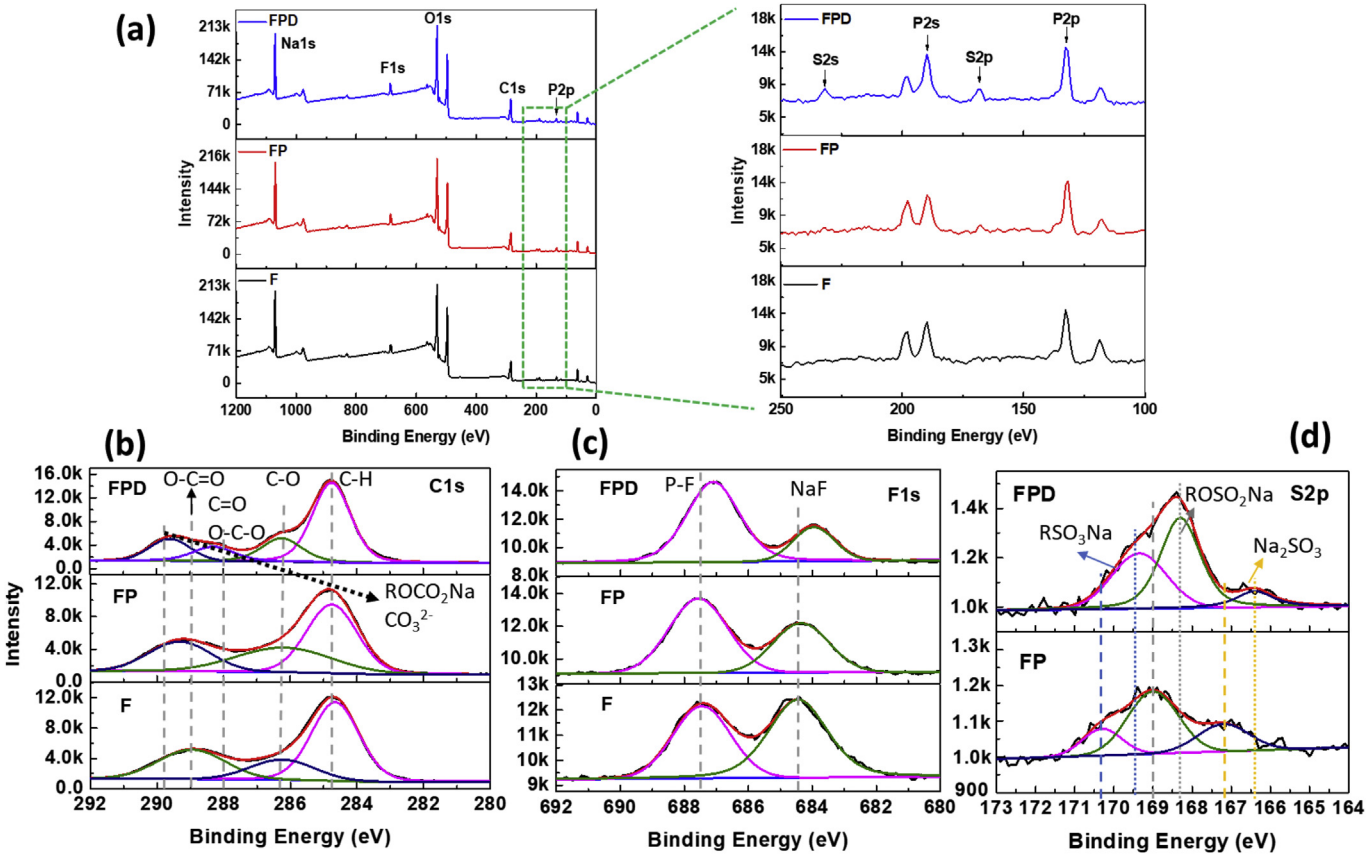

Fig. 4. XPS spectra of cycled HC anode. (a) Overview, (b) C1s spectrum, (c) F1s spectrum, and (d) S2p spectrum.

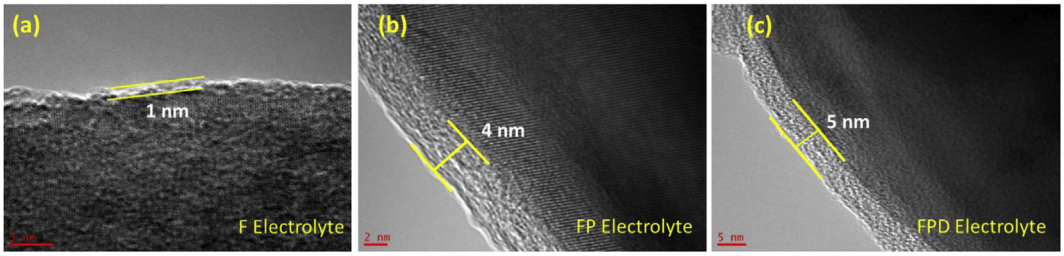

Fig. 5. TEM image of cycled NFM cathodes. (a) Single additive F, (b) bi-additive FP, and (c) tri-additive FPD.

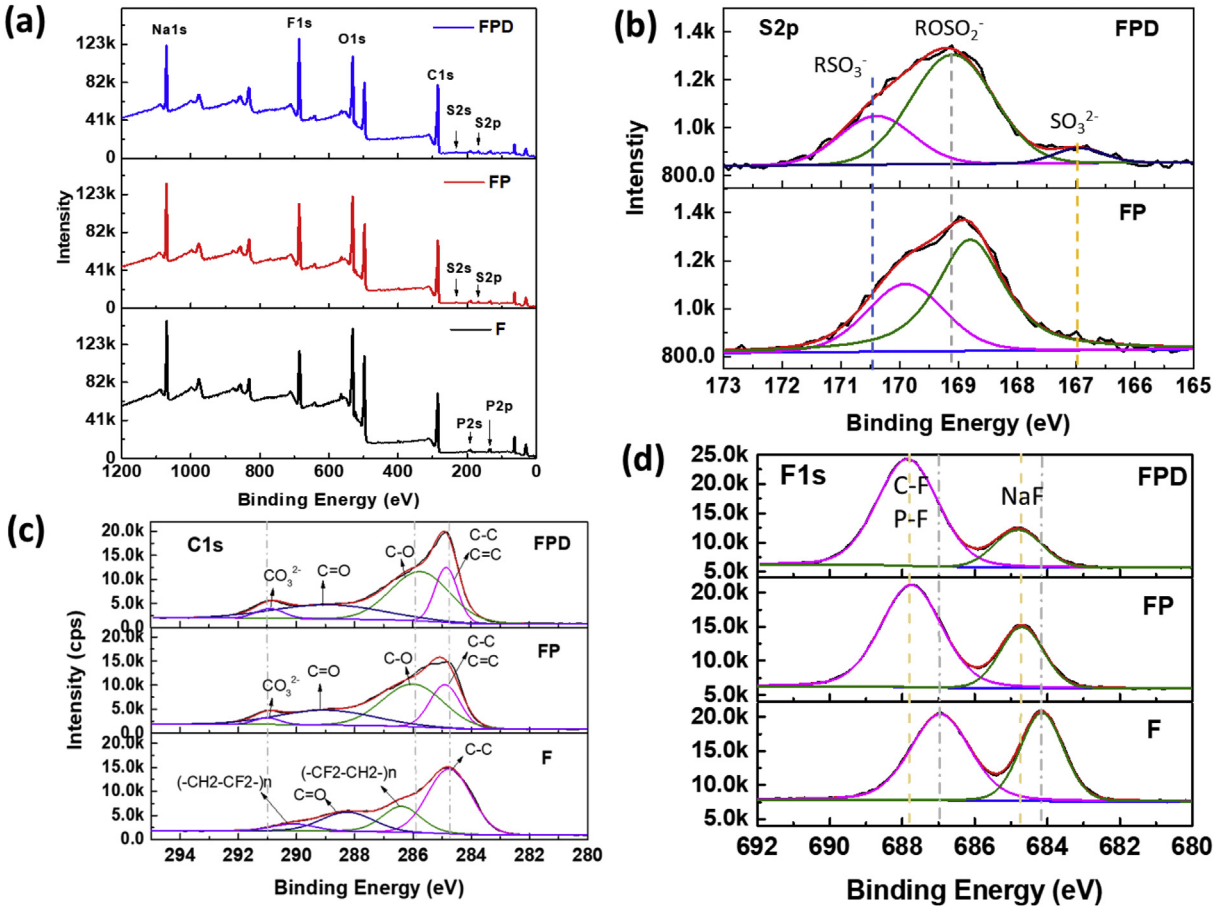

Fig. 6. XPS spectra of cycled NFM cathode. (a) Overview, (b) S2p spectrum, (c) C1s spectrum, and (d) F1s spectrum.

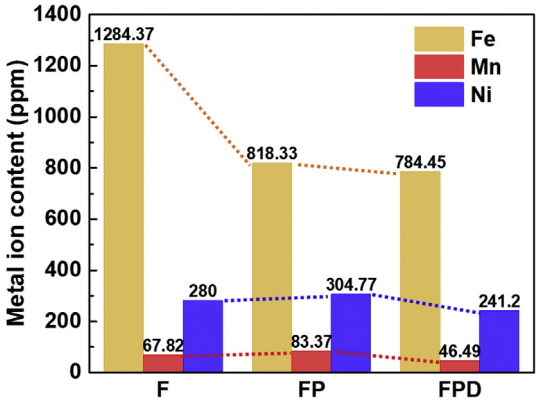

Fig. 7. Effect of electrolyte additive on the dissolution of transition metal ions.

TEM. Fig. 5 shows the TEM images of three NFM cathodes after 1000 cycles in different electrolytes. It is shown that the CEIs formed with FP and FPD multi-additives are much denser and thicker than that formed with the FEC single additive, i.e., about 4–5 nm versus 1 nm in thickness. The dense and thick CEIs formed with the FP or FPD multi-additive not only prevent the oxidation of electrolyte solvents on the cathode but also suppress the dissolution of transition metal ions into the electrolyte.

The XPS spectra of the cycled cathode are indicated in Fig. 6. Similar with the case of the cycled anode, the surface of the cycled cathode contains Na, F, O, C, P, and S elements (Fig. 6a). Comparing the relative intensity of the major peaks in each of detailed spectra, one sees that the bi-additive FP and tri-additive FPD considerably increase the population of the inorganic CO_3^{2-} ions (Fig. 6c, C1s) and organic (covalent) F (Fig. 6d, F1s). In particular, the S2p spectrum (Fig. 6b) shows that there are strong peaks relating to RSO_3^-, $ROSO_2^-$, and SO_3^{2-} species, which are no doubt resulted from PST and DTD molecules in spite of the small difference in their relative intensity between the bi- and tri-additives.

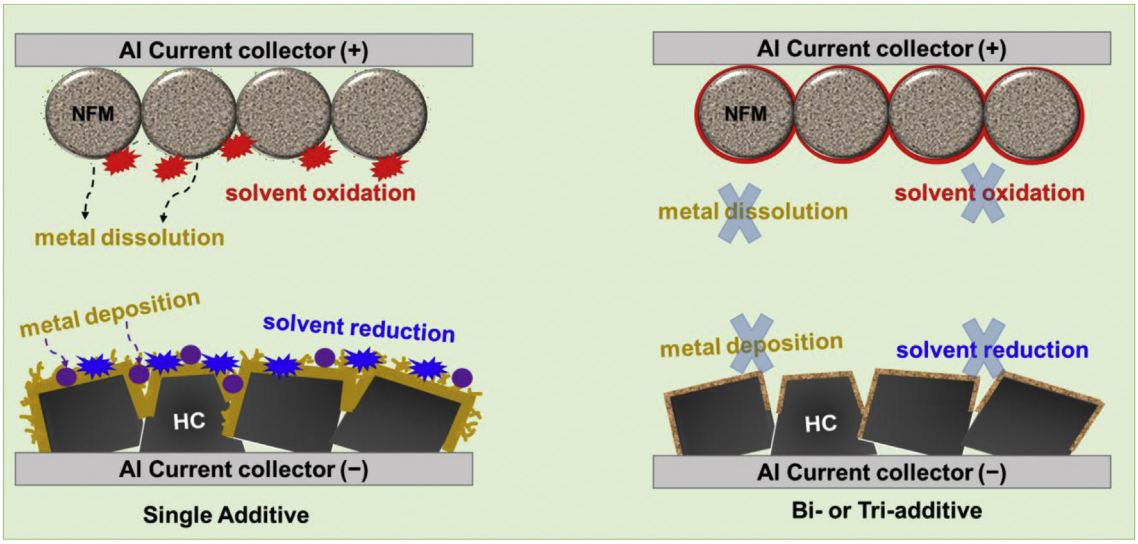

Fig. 8. Schematic summary on the role of PST and DTD additives in HC/NFM full cell.

The unique of the bi- and tri-additives is further reflected in the effect to suppress the dissolution of transition metal ions of the NFM cathode material. Fig. 7 compares the concentrations of Fe, Mn, and Ni ions. It can be seen that Fe ion has the severest dissolution, and that the bi- and tri-additives most effectively suppress the dissolution of Fe ion as compared with the Mn and Ni ions. In particular, the concentration of Fe ions is considerably reduced to 818 ppm and 784 ppm by the FP bi-additive and FPD tri-additive, respectively, as compared with 1284 ppm of the FEC single additive. As suggested by the XPS results of the cycled cathode, the suppression of transition metal dissolution by the bi- and tri-additives can be attributed to the fact that PST and DTD molecules are decomposed on the cathode to RSO_3^-, $ROSO_2^-$ and SO_3^{2-} anions, which subsequently combine with transition metal ions (M^{2+}, M = Fe, Mn, and Ni) to form insoluble transition metal sulfates or sulfites. The resulting compounds are constituted to a dense and much thick CEI, as indicated by Fig. 5b, which prevents further dissolution of the transition metal ions.

Based on the above discussion, the particular functions of PST and DTD molecules in the bi- and tri-additives can be schematically illustrated by Fig. 8. On the HC anode, the PST and DTD molecules promote the formation of a robust SEI by producing more organic molecular moieties, such as $ROCO_2Na$, $ROSO_2Na$, and RSO_3Na, which consequently reduces irreversible reduction (decomposition) of the electrolyte solvents. On the NFM cathode, the PST and DTD molecules decompose to RSO_3^-, $ROSO_3^-$ and SO_3^{2-} anions that subsequently combine with the transition metal ions to form insoluble transition metal sulfates or sulfites, leading to a dense and thick CEI that not only suppresses irreversible oxidation of the electrolyte solvents but also prevents further dissolution of the transition metal ions.

4. Conclusions

Up to 1000 cycles of 1 Ah sodium-ion pouch cells were demonstrated by using a $NaNi_{1/3}Fe_{1/3}Mn_{1/3}O_2$/hard-carbon chemistry and multiple additives that combine fluoroethylene carbonate (FEC) with prop-1-ene-1,3-sultone (PST), or with PST and 1,3,2-dioxathiolane-2,2-dioxide (DTD). Using an optimized electrolyte consisting of 1 M $NaPF_6$ dissolved in 1:1 (vol.) PC-EMC + 2 wt% FEC, 1 wt% PST, and 1 wt% DTD, the pouch cell retained as high as 92.2% capacity retention after 1000 cycles at 1C between 2.0 V and 3.8 V. Post-mortem analyses on the cycled electrodes indicate that PST and DTD additives are able to promote the formation of a robust SEI on the anode by producing more organic molecular moieties, and prevent the dissolution of transition metal ions by inducing to form a dense and thick CEI on the cathode. The results of this work show that using multi-additives is a simple and promising approach for the development of practically viable sodium-ion batteries.

Acknowledgments

This work was supported by the Natural Science Foundation of China (21676165, 21336003, 21573147 and 21506123), the National Key Research and Development Program (2016YFB0901500). The XPS measurements were performed by Mrs. Qianqian Hu in Instrumental Analysis Center of SJTU.

References

[1] H. Pan, Y.S. Hu, L. Chen, Energy Environ. Sci. 6 (2013) 2338–2360.
[2] M.D. Slater, D. Kim, E. Lee, C.S. Johnson, Adv. Funct. Mater. 23 (2013) 947–958.
[3] N. Yabuuchi, K. Kubota, M. Dahbi, S. Komaba, Chem. Rev. 114 (2014) 11636–11682.
[4] M. Sawicki, L.L. Shaw, RSC Adv. 5 (2015) 53129–53154.
[5] J.Y. Hwang, S.T. Myung, Y.K. Sun, Chem. Soc. Rev. 46 (2017) 3529–3614.
[6] Y. Lu, L. Wang, J. Cheng, J.B. Goodenough, Chem. Commun. 48 (2012) 6544–6546.
[7] D. Kim, E. Lee, M. Slater, W. Lu, S. Rood, C.S. Johnson, Electrochem. Commun. 18 (2012) 66–69.
[8] M. Sathiya, K. Hemalatha, K. Ramesha, J.M. Tarascon, A.S. Prakash, Chem. Mater. 24 (2012) 1846–1853.
[9] P. Vassilaras, A.J. Toumar, G. Ceder, Electrochem. Commun. 38 (2014) 79–81.
[10] Y. Liu, X. Fang, A. Zhang, C. Shen, Q. Liu, H.A. Enaya, C. Zhou, Nanomater. Energy 27 (2016) 27–34.
[11] M. Reynaud, A. Wizner, N.A. Katcho, L.C. Loaiza, M. Galceran, J. Carrasco, T. Rojo, M. Armand, M. Casas-Cabanas, Electrochem. Commun. 84 (2017) 14–18.
[12] Y.L. Ruan, K. Wang, S.D. Song, X. Han, B.W. Cheng, Electrochim. Acta 160 (2015) 330–336.
[13] H.J. Song, J. Kim, M.A. Dar, D.W. Kim, J. Power Sources 377 (2018) 121–127.
[14] J. Barker, M.Y. Saidi, J.L. Swoyer, Electrochem. Solid state Lett. 6 (2003) A1 − A4.
[15] A. Ponrouch, R. Dedryvère, D. Monti, A.E. Demet, J.M. Ateba Mba, L. Croguennec, C. Masquelier, P. Johansson, M.R. Palacín, Energy Environ. Sci. 6 (2013) 2361–2369.
[16] M. Nose, H. Nakayama, K. Nobuhara, H. Yamaguchi, S. Nakanishi, H. Iba, J. Power Sources 234 (2013) 175–179.
[17] S. Komaba, W. Murata, T. Ishikawa, N. Yabuuchi, T. Ozeki, T. Nakayama, A. Ogata, K. Gotoh, K. Fujiwara, Adv. Funct. Mater. 21 (2011) 3859–3867.
[18] G.L. Xu, R. Amine, A. Abouimrane, H. Che, M. Dahbi, Z.F. Ma, I. Saadoune, J. Alami, W.L. Mattis, F. Pan, Z. Chen, K. Amine, Adv. Energy Mater. 8 (2018) 1702403.
[19] H. Che, S. Chen, Y. Xie, H. Wang, K. Amine, X. Liao, Z.F. Ma, Energy Environ. Sci. 10 (2017) 1075–1101.
[20] H.S. Lee, Z.F. Ma, X.Q. Yang, X. Sun, J. McBreen, J. Electrochem. Soc. 151 (2004) A1429–A1435.
[21] S. Komaba, T. Ishikawa, N. Yabuuchi, W. Murata, A. Ito, Y. Ohsawa, ACS Appl. Mater. Interfaces 3 (2011) 4165–4168.
[22] U. Purushotham, N. Takenaka, M. Nagaoka, RSC Adv. 6 (2016) 65232–65242.

[23] H. Kumar, E. Detsi, D.P. Abraham, V.B. Shenoy, Chem. Mater. 28 (2016) 8930–8941.
[24] L. Yu, L.P. Wang, S. Xi, P. Yang, Y. Du, M. Srinivasan, Z.J. Xu, Chem. Mater. 27 (2015) 5340–5348.
[25] Z. Huang, H. Hou, G. Zou, J. Chen, Y. Zhang, H. Liao, S. Li, X. Ji, Electrochim. Acta 214 (2016) 156–164.
[26] P.C. Rath, J. Patra, D. Saikia, M. Mishra, J.K. Chang, H.M. Kao, J. Mater. Chem. 4 (2016) 14222–14233.
[27] K. Vignarooban, R. Kushagra, A. Elango, P. Badami, B.E. Mellander, X. Xu, T.G. Tucker, C. Nam, A.M. Kannan, Int. J. Hydrogen Energy 41 (2016) 2829–2846.
[28] B. Li, M. Xu, T. Li, W. Li, S. Hu, Electrochem. Commun. 17 (2012) 92–95.
[29] L. Madec, J. Xia, R. Petibon, K.J. Nelson, J.P. Sun, I.G. Hill, J.R. Dahn, J. Phys. Chem. C 118 (2014) 29608–29622.
[30] J. Xia, N.N. Sinha, L.P. Chen, J.R. Dahn, J. Electrochem. Soc. 161 (2013) A264 – A274.
[31] H. Che, J. Liu, H. Wang, X. Wang, S.S. Zhang, X.Z. Liao, Z.F. Ma, Electrochem. Commun. 83 (2017) 20–23.
[32] H. Wang, X.Z. Liao, Y. Yang, X. Yan, Y.S. He, Z.F. Ma, J. Electrochem. Soc. 163 (2016) A565 – A570.
[33] R.A. Quinlan, Y.C. Lu, D. Kwabi, Y. Shao-Horn, A.N. Mansour, J. Electrochem. Soc. 163 (2015) A300 – A308.
[34] M.A. Munoz-Marquez, M. Zarrabeitia, E. Castillo-Martinez, A. Eguia-Barrio, T. Rojo, M. Casas-Cabanas, ACS Appl. Mater. Interfaces 7 (2015) 7801–7808.